

# Aluminum Incorporation and Interfacial Structures in MCM-41 Mesoporous Molecular Sieves

M. T. Janicke,<sup>†,§</sup> C. C. Landry,<sup>‡,⊥</sup> S. C. Christiansen,<sup>†</sup> D. Kumar,<sup>‡,||</sup> G. D. Stucky,<sup>‡</sup> and B. F. Chmelka<sup>\*,†</sup>

Contribution from the Department of Chemical Engineering and Department of Chemistry, Materials Research Laboratory, University of California, Santa Barbara, California 93106

Received July 31, 1997. Revised Manuscript Received May 4, 1998

**Abstract:** Two-dimensional (2D) solid-state NMR spectroscopy has been used to identify interfacial species and establish framework locations of aluminum atoms incorporated in aluminosilicate MCM-41 mesophases and mesoporous solids. In these experiments, chemical shifts of protons in the material are correlated with the chemical shifts of nearby (ca. 1 nm) <sup>13</sup>C, <sup>27</sup>Al, or <sup>29</sup>Si species via their respective heteronuclear dipole–dipole couplings. For aluminosilicate MCM-41 mesophases prepared at room temperature, 2D heteronuclear chemical shift correlation NMR spectra show that tetrahedrally coordinated aluminum and silicon species are in close spatial proximity to the trimethylammonium head groups of the cationic surfactant species in the as-synthesized materials and to ammonium cations following calcination and ion exchange. For MCM-41 materials synthesized under hydrothermal conditions, 2D heteronuclear correlation NMR measurements show that the appearance of six-coordinate aluminum species results from strongly bound water molecules coordinated to aluminum atoms that are also proximate to the surfactant species. The detection of couplings between <sup>27</sup>Al or <sup>29</sup>Si species and protons associated with the structure-directing surfactant molecules or exchangeable ammonium counterions establishes that a significant fraction of the aluminum atoms are present in the inorganic frameworks of these materials.

## Introduction

Following the announcement of the novel class of mesoporous M41S molecular sieves by Mobil researchers,<sup>1–5</sup> diverse and burgeoning interest has occurred in the use of structure-directing surfactant molecules to organize a variety of metal oxide networks into mesoscopically ordered composite materials with different morphologies. After polymerization of the inorganic components and subsequent calcination treatment to remove the surfactant species, robust metal oxide frameworks can remain intact to yield mesoscopically ordered pore systems. A few examples include mesoporous materials with morphologies in the form of hexagonal arrays (MCM-41, SBA-2, SBA-3, SBA-12, SBA-15), cubic structures (MCM-48, SBA-1, SBA-11, SBA-

13, SBA-16), or the ordered stacking of lamellae (pillared clays, MCM-50).<sup>1–9</sup> The hexagonal and cubic structures generally lead to arrays of pores with a narrow distribution of sizes ( $\pm 0.1$  nm fwhm), which are collectively adjustable according to the characteristic dimension established primarily by the vestigial organic species. In particular, pore sizes can be adjusted by changing the length of the alkyl chains of the surfactant molecules or by adding swelling agents into the hydrophobic regions of the organic phase. The resultant mesoporous materials are characterized by long-range periodicity in the arrangements of the pores or lamellae, with locally disordered inorganic frameworks thus far observed to date.

As the variety of chemical systems and structural morphologies has expanded, much effort has been focused on the substitution of heteroatoms, particularly aluminum, into primarily siliceous frameworks to modify the composition of the inorganic walls.<sup>1–5,10–26</sup> This objective has benefited significantly from recent progress in understanding the molecular

\* To whom correspondence should be addressed.

<sup>†</sup> Department of Chemical Engineering.

<sup>‡</sup> Present address: Institut für Anorganische Chemie, Universität Frankfurt, 60439 Frankfurt, Germany.

<sup>§</sup> Department of Chemistry.

<sup>⊥</sup> Present address: Department of Chemistry, University of Vermont, Burlington, VT 05405.

<sup>||</sup> Present address: Instituto de Tecnología Química, Universidad Politécnica, 46071 Valencia, Spain.

(1) Degnan, T. F.; Johnson, I. D.; Keville, K. M. U.S. Patent No. 5,156,828, 1992.

(2) Kresge, C. T.; Leonowicz, M. E.; Roth, W. J.; Vartuli, J. C.; Beck, J. S. *Nature (London)* **1992**, 359, 710–712.

(3) Beck, J. S.; Vartuli, J. C.; Roth, W. J.; Leonowicz, M. E.; Kresge, C. T.; Schmitt, K. D.; Chu, C. T.-W.; Olson, D. H.; Sheppard, E. W.; McCullen, S. B.; Higgins, J. B.; Schlenker, J. L. *J. Am. Chem. Soc.* **1992**, 114, 10834–10843.

(4) Vartuli, J. C.; Kresge, C. T.; Leonowicz, M. E.; Chu, A. S.; McCullen, S. B.; Johnson, I. D.; Sheppard, E. W. *Chem. Mater.* **1994**, 6, 2070–2077.

(5) Vartuli, J. C.; Schmitt, K. D.; Kresge, C. T.; Roth, W. J.; Leonowicz, M. E.; McCullen, S. B.; Hellring, S. D.; Beck, J. S.; Schlenker, J. L.; Olson, D. H.; Sheppard, E. W. *Chem. Mater.* **1994**, 6, 2317–2326.

(6) Monnier, A.; Schüth, F.; Huo, Q.; Kumar, D.; Margolese, D.; Maxwell, R. S.; Stucky, G. D.; Krishnamurty, M.; Petroff, P.; Firouzi, A.; Janicke, M.; Chmelka, B. F. *Science* **1993**, 261, 1299–1303.

(7) Huo, Q.; Margolese, D. I.; Stucky, G. D. *Chem. Mater.* **1996**, 8, 1147–1160.

(8) Zhao, D.; Feng, J.; Huo, Q.; Melosh, N.; Fredrickson, G. H.; Chmelka, B. F.; Stucky, G. D. *Science* **1998**, 279, 548–552.

(9) Zhao, D.; Huo, Q.; Feng, J.; Chmelka, B. F.; Stucky, G. D. *J. Am. Chem. Soc.* In press.

(10) Kolodziejewski, W.; Corma, A.; Navarro, M.-T.; Pérez-Pariente, J. *Solid State Nucl. Magn. Reson.* **1993**, 2, 253–259.

(11) Chen, C.-Y.; Li, H.-X.; Davis, M. E. *Microporous Mater.* **1993**, 2, 17–26.

(12) Chen, C.-Y.; Burkett, S. L.; Li, H.-X.; Davis, M. E. *Microporous Mater.* **1993**, 2, 27–34.

(13) Janicke, M.; Kumar, D.; Stucky, G. D.; Chmelka, B. F. *Stud. Surf. Sci. Catal.* **1994**, 84, 243–250.

mechanisms by which such inorganic–organic M41S-type mesophases form.<sup>27,28</sup> This occurs through a cooperative process that involves charge-density matching between the charged head groups of amphiphilic molecules and charged inorganic ions. Lamellar, hexagonal, or bicontinuous cubic liquid crystal phases may form if conditions are used that allow self-assembly without polymerization of the inorganic or organic components. For silicate-surfactant systems under highly alkaline conditions, thermodynamically stable lyotropic liquid crystalline behavior may be observed over a relatively wide range of temperatures and compositions, as established by *in situ* <sup>2</sup>H nuclear magnetic resonance spectroscopy (NMR), X-ray diffraction (XRD), and polarized optical microscopy measurements.<sup>28</sup> For conditions that induce self-assembly and rapid concurrent polymerization of the inorganic species, mesoscopic organization can still be produced, though liquid crystalline properties will in general not be observed. Although the same underlying physics are expected to govern self-assembly under such conditions, transient polymerization kinetics modify the processes, and, if sufficiently rapid, result in diminished molecular mobilities that are below those needed for liquid crystalline behavior. This is the regime in which most mesoporous materials syntheses published thus far reside, including those incorporating aluminum into siliceous M41S frameworks. Nevertheless, the well-established physicochemical foundations of liquid crystal self-assembly processes permit appreciable morphological and compositional control of these materials over molecular, mesoscopic, and macroscopic length scales.

As in zeolite systems, aluminum incorporation is of special interest because of the beneficial effects it is anticipated to have on the chemical reaction properties of M41S materials. It is known that substitution of tetrahedral aluminum atoms into a silicate framework requires the accompanying introduction of extra-framework charge-compensating cations, and that these cationic species can impart desirable adsorption and catalytic behaviors to porous aluminosilicates.<sup>29</sup> In the as-synthesized materials, these exchangeable cations can be the head groups of surfactant molecules or other cations, such as sodium, available in the synthesis gel. During calcination, the surfactant or other organic cationic molecules decompose, leaving charge-

compensating alkyl ammonium or proton species as Lewis or Brønsted acid sites in the calcined mesoporous product. These or other cationic species compensate the negative framework charges associated with tetrahedral Al sites in the polymerized and calcined aluminosilicate framework and can be subsequently ion exchanged, if desired.

With the goal of optimizing the composition and properties of aluminum-containing mesoporous solids, it must first be determined to what extent the aluminum has been incorporated into the polymerized inorganic walls. Generally, the extent of aluminum substitution has been measured by <sup>27</sup>Al magic-angle spinning (MAS) NMR to quantify the relative amounts of tetrahedral and octahedral aluminum. On the basis of previous experience from highly crystalline zeolites, it is usually presumed that tetrahedrally coordinated aluminum atoms are incorporated into the silicate walls as desirable framework sites, while octahedrally coordinated aluminum atoms reflect potential extra-framework species that are occluded in the pores or exist as an amorphous byproduct.<sup>10–12,15,17–20,24,25,30</sup> This hypothesis, however, remains untested and of uncertain validity for aluminosilicate solids with noncrystalline framework structures, such as characteristic of the inorganic walls of M41S mesoporous materials. In several sol–gel systems, for example, four-, five-, and six-coordinate “framework” aluminum species have been observed by <sup>27</sup>Al MAS NMR in structurally amorphous gels during crystallization of aluminosilicate minerals (e.g., mul-lite).<sup>31,32</sup>

Previous <sup>27</sup>Al NMR and XRD results have shown that aluminosilicate MCM-41 can be prepared with a distribution of spectroscopically resolved octahedral and tetrahedral aluminum species in noncrystalline environments.<sup>13</sup> In addition, this study suggested that the octahedral aluminum sites could be converted into species with tetrahedral coordination upon calcination. This is consistent with aluminum atoms that are tetrahedrally coordinated within the inorganic framework, but which are interacting strongly with surfactant molecules or adsorbed water to produce aluminum species with effectively octahedral coordination in the as-synthesized material. A similar situation has been observed in nanoporous aluminophosphate materials, such as VPI-5, in which adsorbed water coordinates with framework aluminum to produce octahedral aluminum sites.<sup>33–35</sup> In addition to this ambiguity of whether six-coordinated aluminum species is extra-framework or not, Kloetstra and co-workers have shown that separate dense, aluminum-rich phases can be produced in mesoporous material syntheses with exclusively tetrahedrally coordinated aluminum atoms.<sup>21</sup> On the basis of these observations, presumptions concerning the coordination of framework and extra-framework aluminum species appear to have a weak foundation for the M41S family of mesoporous materials. Consequently, under these circumstances 1D MAS <sup>27</sup>Al NMR measurements must be considered to yield ambiguous results, because the location of aluminum species cannot be inferred from chemical shift assignments to different aluminum bonding symmetries alone. The local environments of the aluminum species must be determined

(14) Schmidt, R.; Akporiaye, D.; Stöcker, M.; Ellestad, O. H. *Stud. Surf. Sci. Catal.* **1994**, *84*, 61–68.

(15) Schmidt, R.; Akporiaye, D.; Stöcker, M.; Ellestad, O. H. *J. Chem. Soc., Chem. Commun.* **1994**, *12*, 1493–1494.

(16) Huo, Q.; Margolese, D. I.; Ciesla, U.; Demuth, D. G.; Feng, P.; Gier, T. E.; Sieger, P.; Firouzi, A.; Chmelka, B. F.; Schüth, F.; Stucky, G. D. *Chem. Mater.* **1994**, *6*, 1176–1191.

(17) Luan, Z.; Cheng, C.-F.; Zhou, W.; Klinowski, J. *J. Phys. Chem.* **1995**, *99*, 1018–1024.

(18) Mokaya, R.; Jones, W. *Chem. Commun.* **1997**, *22*, 2185–2186.

(19) Luan, Z.; Cheng, C.-F.; He, H.; Klinowski, J. *J. Phys. Chem.* **1995**, *99*, 10590–10593.

(20) Borade, R. B.; Clearfield, A. *Catal. Lett.* **1995**, *31*, 267–272.

(21) Kloetstra, K. R.; Zandbergen, H. W.; van Bekkum, H. *Catal. Lett.* **1995**, *33*, 157–163.

(22) Fu, G.; Fyfe, C. A.; Schwiager, W.; Kokotailo, G. T. *Angew. Chem. Int. Ed. Engl.* **1995**, *34*, 1499–1502.

(23) Busio, M.; Jänchen, J.; van Hooff, J. H. C. *Microporous Mater.* **1995**, *5*, 211–218.

(24) Schmidt, R.; Junggreen, H.; Stöcker, M. *J. Chem. Soc., Chem. Commun.* **1996**, *7*, 875–876.

(25) Reddy, K. M.; Song, C. *Catal. Lett.* **1996**, *36*, 103–109.

(26) Ryoo, R.; Ko, C. H.; Howe, R. F. *Chem. Mater.* **1997**, *9*, 1607–1613.

(27) Firouzi, A.; Kumar, D.; Bull, L. M.; Besier, T.; Sieger, P.; Huo, Q.; Walker, S. A.; Zasadzinski, J. A.; Glinka, C.; Nicol, J.; Margolese, D.; Stucky, G. D.; Chmelka, B. F. *Science* **1995**, *267*, 1138–1143.

(28) Firouzi, A.; Atef, F.; Oertli, A. G.; Stucky, G. D.; Chmelka, B. F. *J. Am. Chem. Soc.* **1997**, *119*, 3596–3610.

(29) Breck, D. W. *Zeolite Molecular Sieves: Structure, Chemistry, and Use*; Robert E. Krieger Publishing Co.: Malabar, FL, 1984.

(30) Kosslick, H.; Lischke, G.; Walther, G.; Storek, W.; Martin, A.; Fricke, R. *Microporous Mater.* **1997**, *9*, 13–33.

(31) Komarneni, S.; Roy, R.; Fyfe, C. A.; Kennedy, G. J.; Strobl, H. J. *Am. Ceram. Soc.* **1986**, *69*, C42–C44.

(32) Gerardin, C.; Sundaresan, S.; Benziger, J.; Navrotsky, A. *Chem. Mater.* **1994**, *6*, 160–170.

(33) McCusker, L. B.; Baerlocher, C.; Jahn, E.; Bülow, M. *Zeolites* **1991**, *11*, 308–313.

(34) Fyfe, C. A.; Grondy, H.; Mueller, K. T.; Wong-Moon, K. C.; Markus, T. *J. Am. Chem. Soc.* **1992**, *114*, 5876–5878.

(35) Wu, Y.; Chmelka, B. F.; Pines, A.; Davis, M. E.; Grobet, P. J.; Jacobs, P. A. *Nature (London)* **1990**, *346*, 550–552.

beyond simply establishing different coordinations of the aluminum atoms to distinguish between framework and extra-framework species.

Identifying spatially adjacent molecular species, such as surfactant molecules in proximity to framework aluminum atoms, however, can distinguish between interfacial and non-interfacial species and thus discriminate between framework and extra-framework aluminum atoms. One powerful approach for obtaining this information is through the use of versatile multidimensional solid-state NMR techniques, particularly heteronuclear chemical shift NMR correlation experiments, which identify neighboring atomic species that are separated by ca. 1 nm through their dipole–dipole couplings. For the aluminosilicate mesophase materials of interest here, multidimensional solid-state NMR experiments based on dipolar couplings between protons and  $^{27}\text{Al}$  or  $^{29}\text{Si}$  atoms are used to identify specific protonated species that are adjacent to aluminum and silicon atoms in the material. The thin (ca. 1 nm) aluminosilicate walls of MCM-41 frameworks<sup>6</sup> provide the advantage that essentially all framework Al and Si atoms occupy positions at or very near the inorganic–organic interface. By establishing the existence of dipole–dipole interactions between  $^{27}\text{Al}$  nuclei and protons associated with the structure-directing surfactant molecules, incorporation of aluminum species in the inorganic mesophase framework can for the first time be established unambiguously.

## Experimental Section

**Syntheses of Aluminosilicate MCM-41.** Aluminosilicate MCM-41 materials with comparable molar Si/Al ratios were synthesized under ambient and hydrothermal conditions using aluminum isopropoxide ( $\text{Al}(\text{O}^i\text{Pr})_3$ , Aldrich), sodium hydroxide (Fischer) or tetramethylammonium hydroxide (Aldrich), and cetyltrimethylammonium bromide (CTAB, Aldrich) as precursor agents. For the samples prepared under ambient reaction conditions, tetraethoxysilane (TEOS, Fluka) was used as the silica source; for the hydrothermal synthesis, CAB-O-SIL M-5 (Scintillation grade, Kodak) and sodium silicate (N brand, P. Q. Corporation) were used. At room temperature, the aluminosilicate MCM-41a, synthesized under *ambient* conditions, was prepared from a reaction mixture with the following molar gel composition: 1.00  $\text{Al}(\text{O}^i\text{Pr})_3$ :847  $\text{H}_2\text{O}$ :4.33  $\text{NaOH}$ :0.95  $\text{CTAB}$ :8.00  $\text{SiO}_2$ . Initially, 0.472 g of  $\text{Al}(\text{O}^i\text{Pr})_3$  was mixed with 39.2 g of deionized water and 5.00 g of 2 M  $\text{NaOH}$  solution and stirred for 1 h. This fully dissolved the aluminum precursor, providing monomeric aluminum species in the solution. Subsequently, 0.80 g of CTAB was added to this clear solution, and the mixture was slightly heated to dissolve the surfactant. Finally, 3.85 g of TEOS was added as the source of silica to the solution, and the mixture was stirred for 16 h at room temperature. During this time, condensation of the silica and alumina monomers occurs, after which the final polymerized product was filtered and washed before sample characterization.

Under certain conditions, hydrothermal syntheses of aluminosilicate MCM-41 have been shown previously to yield a significant fraction of octahedrally coordinated aluminum in the mesophase product prior to calcination.<sup>13</sup> To characterize the Al species in these materials, aluminosilicate MCM-41 was prepared under *hydrothermal* conditions (MCM-41h) from a reaction mixture with a molar Si/Al ratio of 6/1 and the following molar composition: 1.00  $\text{Al}(\text{O}^i\text{Pr})_3$ :338  $\text{H}_2\text{O}$ :2.0  $(\text{CH}_3)_4\text{NOH}$  (TMAOH):1.67  $\text{CTAB}$ :6.00  $\text{SiO}_2$ . TMAOH was used instead of  $\text{NaOH}$  to regulate the pH in the hydrothermal preparation because under such conditions the presence of  $\text{Na}^+$  cations was observed to yield zeolite A as an unwanted side product. Preparation of this sample was identical to that reported previously,<sup>13</sup> except that the aluminum isopropoxide was added to the TMA-silicate, sodium silicate, and water solution and was stirred for 5 min to begin the hydrolysis of the aluminum species before adding the remaining silica and CTAB. Following the addition of the remaining CAB-O-SIL M-5 and the CTAB solution, the mixture was sealed in a Teflon bottle,

shaken vigorously, and statically heated to 100 °C for 24 h before being filtered and washed with deionized water.

Both the ambient and hydrothermally prepared aluminosilicate materials were subjected to careful calcination treatment, as described previously.<sup>13</sup> Using a Lindberg tube furnace and an inert atmosphere of flowing  $\text{N}_2$  or Ar, alumina crucibles containing thin beds of the MCM-41 samples were heated to 500 °C with a 1 °C/min ramp and held at this elevated temperature for 6 h. Subsequently, the samples were cooled at 2 °C/min to room temperature, and the heating procedure was then repeated under flowing  $\text{O}_2$ .

To ensure complete removal of extraneous charge-balancing cations and to provide a proton source for introducing subsequent Brønsted acidity, the final calcined materials were ion-exchanged with  $\text{NH}_4^+$  cations. A 1.0 M  $\text{NH}_4\text{Cl}$  (Fisher) aqueous solution was prepared and pH balanced to 7.0 using concentrated aqueous  $\text{NH}_4\text{OH}$  (Fisher). The MCM-41 samples were added to the aqueous ion-exchange solution (1 mg of MCM-41/1 mL of solution) at room temperature, briefly stirred, and allowed to settle for 1 h. The solution was subsequently decanted, and the ion-exchange process was repeated with fresh  $\text{NH}_4\text{Cl}$  solution. Three ion exchanges in this manner were used to ensure essentially complete exchange. Short ion exchanges were deemed preferable to avoid deterioration of the samples and because the predominant fraction of the materials of primary interest contain large pores with exchangeable ions that can be freely accessed. XRD diffraction patterns confirmed that, under these conditions, the structural integrities of the samples were preserved during the exchange processes. After the final exchange, the samples were filtered, washed with copious amounts of deionized water, and air-dried.

The ammonium-exchanged samples were hydrophilic and were dehydrated under vacuum prior to characterization by NMR. Adsorbed water tended to diminish the spectral resolution of the NMR measurements by overwhelming the  $^1\text{H}$  peaks from the surfactant species of primary interest. Ammonium-exchanged samples were packed into MAS rotors and dehydrated for 48 h at room temperature and at  $10^{-5}$  Torr. Under these conditions, a majority of the physically adsorbed water could be removed without decomposing the  $\text{NH}_4^+$  cations. The rotors were subsequently capped and sealed with epoxy in the dry  $\text{N}_2$  atmosphere of a glovebox. This method provided the highest filling factor for the dry samples in the NMR experiments without resorting to cumbersome sealed glass ampoules.

**Characterization. (a) Elemental Analysis.** Chemical analyses of the MCM-41 aluminosilicate samples were obtained from Galbraith Laboratories (Knoxville, TN) and used to establish bulk Si/Al ratios for the mesophase products.

**(b) X-ray Powder Diffraction.** X-ray powder diffraction (XRD) data were acquired on a Scintag PAD X diffractometer using  $\text{Cu-K}\alpha$  radiation and a liquid nitrogen-cooled germanium solid-state detector. Typically, the data were collected from 1.5° to 10.5° ( $2\theta$ ) with a resolution of 0.02° and a count time of 1.6 s at each point.

**(c) Solid-State NMR.** Solid-state NMR experiments were performed with a Chemagnetics CMX-500 spectrometer using a wide-bore superconducting 11.7 T magnet from Magnex Scientific. Magic-angle spinning (MAS) NMR spectra were obtained using a Chemagnetics MAS probe equipped with 7.5-mm zirconia rotors. The  $^1\text{H}$ ,  $^{13}\text{C}$ , and  $^{29}\text{Si}$  chemical shifts are referenced to TMS, and the  $^{27}\text{Al}$  shifts (which reflect a combination of separate chemical shift and field-dependent second-order quadrupolar shift components) are referenced to a dilute aqueous  $\text{Al}(\text{NO}_3)_3$  solution. Experimental conditions for the individual NMR experiments varied and are presented in detail in the figure captions accompanying the respective spectra.

## Two-Dimensional Chemical Shift Correlation NMR

The technique adapted for this study, HETeronuclear chemical shift CORrelation spectroscopy (HETCOR),<sup>36,37</sup> distinguishes

(36) Ernst, R. R.; Bodenhausen, G.; Wokaun, A. *Principles of Nuclear Magnetic Resonance in One and Two Dimensions*; Oxford University Press: New York, 1994.

(37) Schmidt-Rohr, K.; Spiess, H. W. *Multidimensional Solid-State NMR and Polymers*; Academic Press: San Diego, 1994.

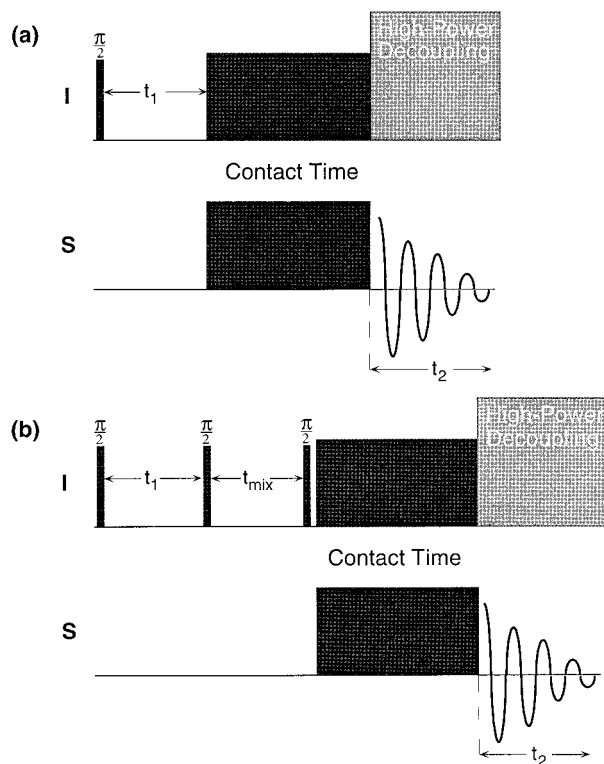


**Figure 1.** Schematic diagrams of pulse sequences for two-dimensional solid-state NMR experiments that correlate the chemical shifts of molecular species that are dipole–dipole coupled to one another. The HETeronuclear chemical shift CORrelation spectroscopy (HETCOR) experiment without (a) and with (b)  $^1\text{H}$  spin diffusion, where  $I$  typically represents  $^1\text{H}$  and  $S$  represents  $^{13}\text{C}$ ,  $^{27}\text{Al}$ , or  $^{29}\text{Si}$ .

between various aluminum (or silicon) species associated with surfactant molecules, adsorbed water, or hydroxyl groups in the M41S synthesis products by correlating specific  $^1\text{H}$  and  $^{27}\text{Al}$  (or  $^1\text{H}$  and  $^{29}\text{Si}$ ) peak positions in a two-dimensional (2D) NMR spectrum. This is achieved by creating  $^1\text{H}$  magnetization during the first time domain of a 2D NMR experiment and transferring it to dipolar-coupled nuclei in close spatial proximity for the second time domain, during which the signal is detected (Figure 1a). Because the necessary dipolar couplings have a strong  $1/r^3$  dependence, where  $r$  is the internuclear distance separating the coupled nuclei, only correlations between neighboring atomic species are observed. This experiment has been described in detail by Vega for  $^1\text{H}$ – $^{29}\text{Si}$  correlation studies of silanol groups in silicas and zeolites.<sup>38</sup> Fyfe and co-workers have used a similar technique for examining heterogeneities in methyl-functionalized silica gels.<sup>39</sup> The heteronuclear chemical shift correlation technique is similar to conventional cross-polarization magic-angle spinning (CPMAS) NMR,<sup>36,40</sup> except that the  $^1\text{H}$  magnetization is allowed to evolve for a period  $t_1$  before the magnetization is transferred to the nuclei of interest, for example,  $^{27}\text{Al}$  or  $^{29}\text{Si}$ .<sup>38</sup> Conducting this as a 2D NMR experiment allows correlations to be made between the chemical shifts for proton species and to spatially proximate  $^{13}\text{C}$ ,  $^{27}\text{Al}$ , or  $^{29}\text{Si}$  atoms. Magnetization is exchanged only between heteronuclear dipole–dipole-coupled species, that is, nuclei separated by less than ca. 1 nm for the short contact times typically used in this study. For this reason, the HETCOR experiment provides detailed and

correlated structural information regarding molecular environments in close proximity to different protonated species, such as structure-directing or charge-compensating molecules that may be interacting strongly with the inorganic MCM-41 framework.

To examine species that experience relatively weak dipole–dipole couplings, it is necessary to extend the time over which the different spin pairs can become correlated. In principle, this can be achieved by lengthening the contact time of the HETCOR experiment (Figure 1a); however, the feasibility of this approach is limited by spin-lattice ( $T_{1\rho}$ ) relaxation of the species involved. This presents particular difficulties for quadrupolar nuclei, such as  $^{27}\text{Al}$  which typically possess short  $T_{1\rho}$  values, on the order of a few hundred microseconds.<sup>41,42</sup> Nevertheless, it is possible to extend the HETCOR method to the study of weakly coupled species with short  $T_{1\rho}$  values by modifying the experiment to allow controlled proton spin diffusion to occur during an added mixing time.<sup>43</sup> The presence of strong homonuclear dipole–dipole interactions among different proton species in a sample serves to extend appreciably the range of molecular distances and mobilities over which, for example,  $^1\text{H}$ – $^{27}\text{Al}$  couplings can be investigated. This is possible because efficient  $^1\text{H}$ – $^1\text{H}$  coupling can be used to mix magnetization among nearby proton species before it is transferred to a nearby  $^{27}\text{Al}$  atom via heteronuclear dipole–dipole interactions. As shown in Figure 1b, this may be implemented by modifying the standard HETCOR experiment (see Figure 1a): an additional  $\pi/2$  pulse is incorporated after the evolution time ( $t_1$ ) to store the  $^1\text{H}$  magnetization along the  $z$ -axis, followed by a mixing time ( $t_{\text{mix}}$ ), during which proton spin diffusion can occur. The diffusion of the proton magnetization during the mixing period can be regulated to occur over distances from 1 to ca. 100 nm, depending on the density of the coupled-proton system, the time ( $t_{\text{mix}}$ ) that the dipolar-coupled species are allowed to interact, and their respective relaxation times.<sup>43–45</sup> As in the standard HETCOR experiment, a contact time is subsequently used to transfer magnetization from the proton nuclei to nearby  $^{27}\text{Al}$  (or other heteronuclear dipole–dipole coupled) species for detection during  $t_2$ . Longer mixing times allow weaker  $^1\text{H}$ – $^{27}\text{Al}$  couplings to be established, with substantial increases in the range over which distance correlations can be measured. Moreover, because short contact times can still be used to transfer magnetization between heteronuclear coupled species, measurement of the weaker couplings is limited predominantly by  $^1\text{H}$   $T_1$  relaxation times (a few hundred milliseconds, which is several orders of magnitude longer than the short  $T_{1\rho}$  values of  $^{27}\text{Al}$ ).

In both the standard HETCOR experiment (Figure 1a) and the spin-diffusion HETCOR variant (Figure 1b), magnetization is transferred between the two nuclei through continuous-wave spin-locking, provided the Hartmann–Hahn matching condition is satisfied. For  $^{13}\text{C}\{^1\text{H}\}$  and  $^{29}\text{Si}\{^1\text{H}\}$  double-resonance MAS experiments, where the first nucleus listed is the observed species and the bracketed nucleus identifies the source of the observed species' magnetization, the modified Hartmann–Hahn

(41) Fyfe, C. A.; Wong-Moon, K. C.; Huang, Y.; Grondey, H.; Mueller, K. T. *J. Phys. Chem.* **1995**, *99*, 8707–8716.

(42) Mortuza, M. G.; Dupree, R.; Kohn, S. C. *Appl. Magn. Reson.* **1993**, *4*, 89–100.

(43) Schmidt-Rohr, K.; Clauss, J.; Spiess, H. W. *Macromolecules* **1992**, *25*, 3273–3277.

(44) VanderHart, D. L.; McFadden, G. B. *Solid State Nucl. Magn. Reson.* **1996**, *7*, 45–66.

(45) Clauss, J.; Schmidt-Rohr, K.; Spiess, H. W. *Acta Polym.* **1993**, *44*, 1–17.

(38) Vega, A. J. *J. Am. Chem. Soc.* **1988**, *110*, 1049–1054.

(39) Fyfe, C. A.; Zhang, Y.; Aroca, P. *J. Am. Chem. Soc.* **1992**, *114*, 3252–3255.

(40) Mehring, M. *Principles of High-Resolution NMR in Solids*; Springer-Verlag: New York, 1983.

**Table 1.** Molar Si/Al Ratios Obtained from Elemental Analyses of Aluminosilicate MCM-41 Materials Prepared under Ambient and Hydrothermal Conditions and Their Respective  $d_{100}$  Spacings, before and after Calcination, Obtained from Powder X-ray Diffraction

sample (synthesis conditions)	molar Si/Al ratio		$d_{hkl}$ spacing ( $\pm 1$ Å)		
	reaction gel	solid product	$hkl$	as-synthesized	calcined
MCM-41a (ambient, 25 °C)	8.0	4.5	100	45.5	39.4
MCM-41h (hydrothermal, 100 °C)	6.0	5.5	100	41.2	39.4

condition for two spin-1/2 nuclei is

$$\gamma_I B_{II} = \gamma_S B_{IS} + n\omega_r \quad (1)$$

where  $I$  generally represents the insensitive abundant nucleus ( $^1\text{H}$ ); and  $S$  is the sensitive dilute nucleus, such as  $^{13}\text{C}$  or  $^{29}\text{Si}$ ;  $\gamma_i$  are the respective gyromagnetic ratios for the different nuclei;  $B_{II}$  are the magnetic fields associated with radio frequency pulses at the Larmor frequencies of the two nuclei; and  $n\omega_r$  is an integer multiple of the rotor frequency  $\omega_r$ .<sup>46,47</sup> Adamantane and tetrakis(trimethyl)silylsilane were used as standards to optimize the Hartmann–Hahn conditions for  $^{13}\text{C}$  and  $^{29}\text{Si}$ , respectively. For the  $^{27}\text{Al}\{^1\text{H}\}$  experiments, the modified Hartmann–Hahn condition takes into account that  $^{27}\text{Al}$  is a quadrupolar nucleus with a nuclear spin of 5/2. In this case, the matching condition for excitation of the  $^{27}\text{Al}$  central transition is<sup>48</sup>

$$\gamma_I B_{II} = 3\gamma_S B_{IS} + n\omega_r \quad (2)$$

Optimizing  $^1\text{H}$  cross-polarization to quadrupolar nuclei is more complicated than similar experiments involving only spin-1/2 nuclei; however, efficient methods for finding the Hartmann–Hahn condition for  $^{27}\text{Al}\{^1\text{H}\}$  CPMAS have been previously reported.<sup>42,49</sup> Kaolinite was used to establish reliable matching conditions for the  $^{27}\text{Al}\{^1\text{H}\}$  HETCOR measurements.<sup>49</sup>

## Results and Discussion

**Bulk Sample Aluminum Contents.** Elemental analyses were performed on aluminosilicate MCM-41 samples synthesized under ambient and hydrothermal conditions to determine the bulk average concentrations of aluminum present in the as-synthesized and calcined products. As determined from elemental analyses, the MCM-41a product prepared at room temperature possessed a higher concentration of aluminum than present in the reaction gel: the bulk molar Si/Al ratio in the solid product was 4.5, nearly double that present in the reaction mixture (Table 1). Similar results were found for other aluminosilicate M41S materials prepared under ambient conditions. The final products consistently contained a lower molar Si/Al ratio than the starting gels until an apparent maximum aluminum loading of approximately unity was reached. Synthesis and characterization of these low silica M41S materials will be discussed in a separate publication.<sup>50</sup>

For the MCM-41 material synthesized under hydrothermal conditions at 100 °C, elemental analyses revealed comparable molar Si/Al ratios in the starting gel (6.0) and the final product

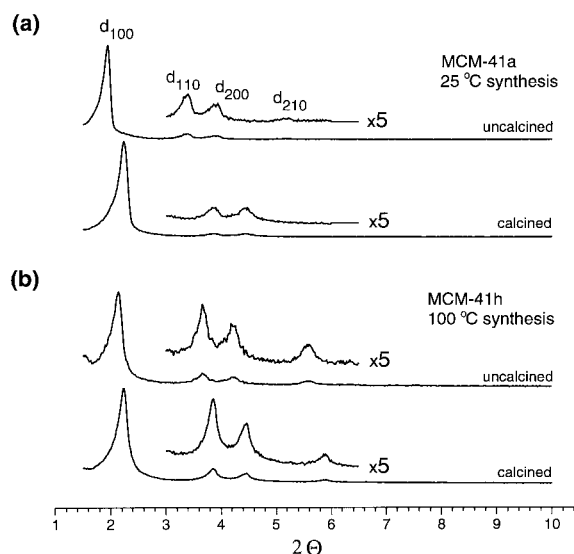


**Figure 2.** X-ray powder diffraction patterns for aluminosilicate MCM-41 materials prepared under (a) ambient (MCM-41a) and (b) hydrothermal (MCM-41h) conditions. Results presented for both as-synthesized and calcined materials show low-angle peaks that are characteristic of hexagonally ordered mesophases. Insets are five times the intensity of the full XRD patterns.

(5.5). Similar results have been observed for MCM-41 materials prepared under hydrothermal conditions with higher Si/Al ratios ranging from 16 to 64.<sup>13</sup> In these previous investigations, elemental analyses and energy-dispersive X-ray spectroscopy (EDX) measurements confirmed that the molar Si/Al ratios were essentially uniform for the bulk samples and over the individual micron-sized MCM-41 particles, respectively. Investigations of the mechanism by which the mesoscopically ordered silicate–surfactant systems are formed have supported the observations that alumina anions that are not fully hydrolyzed, are thus inaccessible during rapid self-assembly, and tend to be excluded from the inorganic–organic composite product.<sup>11,13,27,28</sup> For the hydrothermal syntheses of MCM-41 produced at 100 °C described here, it appears that the rates at which the aluminum and silicon are incorporated into the inorganic framework are similar, resulting in final products that retain the Si/Al ratios of the initial gels.

**Mesophase Morphology Identification: XRD.** Powder X-ray diffraction allows the morphology and mesoscopic order of the aluminosilicate MCM-41 materials to be established, following synthesis and postsynthesis modification (e.g., calcination and ion exchange) of the materials. As shown in Figure 2, both the ambient and hydrothermal syntheses resulted in materials with  $p6mm$  symmetry corresponding to the hexagonal MCM-41 morphology. These XRD patterns are typical for a hexagonal MCM-41 material made using cetyltrimethylammonium (CTA<sup>+</sup>) species as the structure-directing surfactant agent.<sup>2,3,6</sup> For the as-synthesized MCM-41a material prepared at room temperature,  $d_{100}$ ,  $d_{110}$ , and  $d_{200}$  reflections are observed at 46.5, 26.9, and 22.4 Å, respectively, in Figure 2a. The  $d_{210}$  reflection is also present at ca. 17 Å, although its position cannot be accurately determined because its intensity is near the sensitivity limit of the measurement. Similarly, as shown in Figure 2b,  $d_{100}$ ,  $d_{110}$ ,  $d_{200}$ , and  $d_{210}$  reflections occur at 41.2, 24.1, 21.1, and 15.9 Å, respectively, for as-synthesized MCM-41h prepared hydrothermally at 100 °C. The XRD patterns (Figure 2) obtained for the calcined MCM-41a,h materials show that the hexagonal morphologies are preserved, confirmation of the structural stability of the polymerized aluminosilicate

(46) Stejskal, E. O.; Schaefer, J. *J. Magn. Reson.* **1977**, *28*, 105–112.

(47) Schaefer, J.; Stejskal, E. O.; Garbow, J. R.; McKay, R. A. *J. Magn. Reson.* **1984**, *59*, 150–156.

(48) Vega, A. J. *Solid State Nucl. Magn. Reson.* **1992**, *1*, 17–32.

(49) Kolodziejewski, W.; Corma, A. *Solid State Nucl. Magn. Reson.* **1994**, *3*, 177–180.

(50) Janicke, M. T.; Landry, C. C.; Stucky, G. D.; Chmelka, B. F. Manuscript in preparation.

materials, following removal of the structure-directing surfactant molecules. Based on these X-ray diffraction results, the hexagonal morphologies and stabilities of the aluminosilicate MCM-41 products are established.

X-ray diffraction, however, does not provide direct evidence of the extent to which aluminum has been incorporated into the mesoscopically organized inorganic frameworks. In particular, exclusion of aluminum species into disordered extra-framework domains is difficult to detect using scattering techniques. Similarly, while elemental analyses indicate that aluminum is present in the final bulk product, this method likewise cannot distinguish between framework and extra-framework aluminum species. Chemical reaction analyses have provided perhaps the most substantial evidence to date of the effects of aluminum incorporation in MCM-41.<sup>51–53</sup> Nevertheless, from the typically global nature of such reaction measurements, it is generally not possible to obtain direct or detailed information on the structure and location of aluminum species and their accompanying role(s) in explaining the adsorption or reaction properties of mesoporous aluminosilicate solids. Limitations such as these have made it difficult to suitably characterize important structural features of these complicated heterogeneous materials, particularly as related to aluminum incorporation in the inorganic frameworks.

**Characterization of Interfacial Species: 2D Solid-State NMR. (a) Assignment of Proton Resonances.** The presence of framework aluminum species in M41S materials, along with detailed information on their local structure, can however be unambiguously established through the use of 2D HETCOR solid-state NMR studies. This is achieved by measuring dipole–dipole couplings between <sup>27</sup>Al nuclei and protons associated with the cationic head groups of the structure-directing surfactant species or exchangeable NH<sub>4</sub><sup>+</sup> cations. (The higher natural abundance and large gyromagnetic ratio of protons as compared to <sup>13</sup>C make <sup>1</sup>H-containing moieties generally more suitable for measuring HETCOR correlations involving <sup>27</sup>Al and <sup>29</sup>Si; <sup>13</sup>C–<sup>27</sup>Al and <sup>13</sup>C–<sup>29</sup>Si couplings are often weak and averaged away by MAS conditions required to improve sensitivity and resolution.) The existence of <sup>1</sup>H–<sup>27</sup>Al couplings reflects the interfacial locations of the different moieties that permit surface framework Al species to be distinguished from non-interfacial species. Al species that are not associated with the inorganic–organic interface, whether in small domains or in large phase-separated regions, will generally be unable to influence desirable surface reactions within the pores of the MCM-41 product. Here, such aluminum species will be considered to effectively occupy ‘non-framework’ sites.

Two-dimensional <sup>13</sup>C{<sup>1</sup>H} HETCOR experiments on aluminosilicate MCM-41 materials were used first to correlate well-known <sup>13</sup>C NMR resonances from specific organic moieties to their corresponding <sup>1</sup>H NMR peaks. This permitted all protonated species in the mesophase materials to be identified, so that assignments of specific <sup>1</sup>H–<sup>27</sup>Al couplings could be subsequently achieved without ambiguity. Attributing <sup>1</sup>H resonances in solid-state NMR spectra to particular chemical species is often difficult, because the narrow proton chemical shift range and strong homonuclear <sup>1</sup>H–<sup>1</sup>H dipole–dipole couplings cause <sup>1</sup>H peaks to be often overlapping and broad. Magic-angle spinning assists in narrowing the lines by averaging the <sup>1</sup>H

chemical shift anisotropy and dipolar couplings, although often only partially so for typically strong homonuclear <sup>1</sup>H–<sup>1</sup>H interactions. Multidimensional NMR techniques have been used to overcome or mitigate these difficulties by correlating <sup>1</sup>H interactions with neighboring species in one or more additional frequency dimensions, often leading to significantly enhanced spectral resolution. For example, well-resolved resonances from a dilute nucleus, such as <sup>13</sup>C in wideline-separation NMR spectroscopy, have been used to separate overlapping <sup>1</sup>H frequencies into a second dimension in studies of molecular structure and dynamics in polymers.<sup>37,43</sup> In addition, several multiple-pulse NMR experiments, like CRAMPS and WIM24, have been developed to reduce the effects of homonuclear dipolar couplings and thereby improve the resolution of <sup>1</sup>H MAS spectra.<sup>37,54</sup> Such multiple-pulse homonuclear decoupling strategies, however, are not required to resolve individual components in the <sup>1</sup>H MAS spectra for protonated species in the MCM-41 materials under investigation here. Sufficient molecular mobilities and/or internuclear separations apparently exist for the cetyltrimethylammonium species near ambient temperature to produce relatively weak dipolar couplings between <sup>1</sup>H nuclei, so that resolved <sup>1</sup>H MAS spectra are obtained for the different aluminosilicate MCM-41 samples, as shown below.

The advantage presented by 2D heteronuclear correlation NMR experiments is that chemical shifts from dipole–dipole-coupled species are separated into two frequency dimensions, which allows adjacent nuclear species to be readily determined. Figure 3 shows a 2D contour plot of the <sup>13</sup>C{<sup>1</sup>H} HETCOR spectrum obtained from the ambient-prepared MCM-41a sample in which all <sup>13</sup>C magnetization detected has originated and been transferred from nearby protons through their heteronuclear dipolar couplings. The <sup>13</sup>C{<sup>1</sup>H} CPMAS spectrum is plotted along the horizontal axis, and the <sup>1</sup>H MAS spectrum is plotted along the vertical axis. For clarity, projections are not used, so that all resonances can be accounted for, even if certain correlations are absent in the subsequent 2D spectrum. These spectra, including the 2D HETCOR plot, are representative of the MCM-41h sample prepared under hydrothermal conditions as well.

From Figure 3, the <sup>13</sup>C{<sup>1</sup>H} HETCOR experiment establishes that the <sup>1</sup>H peak at 3.2 ppm is clearly correlated to the trimethylammonium <sup>13</sup>C peak at 54 ppm in the <sup>13</sup>C dimension and can thus be assigned to the proton species of the methyl groups attached to the surfactant head group. The <sup>13</sup>C chemical shifts for the alkyl chain carbon species appear in the range from 14 to 33 ppm, and these correlate with their proton species at 1–2 ppm. The methylene carbon atoms' <sup>13</sup>C chemical shifts appearing at 23, 31, and 33 ppm are correlated with the proton resonance at 1.2 ppm. The carbon resonance at 14 ppm is associated with the terminal methyl group on the surfactant tails and is correlated to the proton species at 1.0 ppm. The peak at 5.3 ppm in the <sup>1</sup>H MAS spectrum along the vertical axis is due to adsorbed water. This signal can be diminished by room-temperature dehydration, which improves the spectral resolution in the <sup>1</sup>H dimension, allowing the chemical shifts for the remaining <sup>1</sup>H peaks to be more accurately measured. The peak at 5.3 ppm is restored upon re-exposure to a hydrating atmosphere. Note, the only carbon species that are not accounted for in the 2D <sup>13</sup>C{<sup>1</sup>H} HETCOR spectrum are the  $\alpha$ -carbon atoms adjacent to the surfactant head group on the alkyl chain. The <sup>13</sup>C peak intensity for this site at 67 ppm is significantly diminished because the peak is broader than the other carbon species; however, it can be observed in the <sup>13</sup>C

(51) Corma, A.; Martinez, A.; Martinez-Soria, V.; Monton, J. B. *J. Catal.* **1995**, *153*, 25–31.

(52) Climent, M. J.; Corma, A.; Iborra, S.; Navarro, M. C.; Primo, J. J. *Catal.* **1996**, *161*, 783–789.

(53) Corma, A.; Grande, M. S.; Gonzalez-Alfaro, V.; Orchilles, A. V. *J. Catal.* **1996**, *159*, 375–382.

(54) Burum, D. P.; Bielecki, A. *J. Magn. Reson.* **1991**, *94*, 645–652.

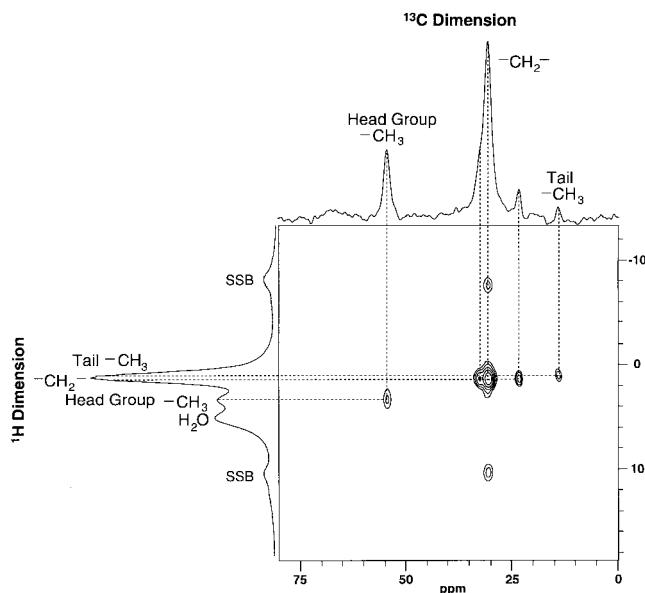


**Figure 3.** 2D  $^{13}\text{C}\{^1\text{H}\}$  HETCOR spectrum for as-synthesized aluminosilicate MCM-41a prepared at room temperature and using a molar Si/Al ratio of 8 in the reaction gel. Separate  $^{13}\text{C}$  CPMAS and  $^1\text{H}$  MAS spectra are plotted along their corresponding axes. In the  $^{13}\text{C}\{^1\text{H}\}$  HETCOR spectrum, cross-peaks associated with chemical shift correlations between  $^{13}\text{C}$  and proton species in the alkyl chains or the trimethylammonium head groups of the surfactant molecules are clearly visible. Spinning sidebands (SSB) from the  $-\text{CH}_2-$   $^1\text{H}$  species are also observed in the  $^1\text{H}$  dimension appearing above and below the isotropic peak at intervals of the MAS rotor speed. This spectrum is representative of all MCM-41 samples prepared under both ambient and hydrothermal conditions.<sup>55</sup> Experimental Conditions: The sample was spun at 4.5 kHz; a 7.5- $\mu\text{s}$   $90^\circ$  pulse followed by a 5-ms contact time was used for cross-polarization. The dwell time in  $t_1$  was 16.7  $\mu\text{s}$ , with the proton signals acquired off-resonance for phase sensitivity. The 640 acquisitions with a 2-s recycle delay were collected for each of the 108  $t_1$  increments. During the detection period ( $t_2$ ), 1024 points were collected with a dwell time of 33.3  $\mu\text{s}$ . The first time domain was subsequently zero-filled to 512 points, and sinebell apodization and 50-Hz Gaussian line broadening were applied in  $t_1$  and  $t_2$ , respectively.

CPMAS spectrum when the number of acquisitions is substantially increased.

Thus, the  $^1\text{H}$  chemical shifts of the proton species in the  $^1\text{H}$  solid-state MAS spectrum of the as-synthesized MCM-41 materials can be identified by using the HETCOR technique to correlate  $^1\text{H}$  peak positions with the  $^{13}\text{C}$  spectral lines associated with the well-established carbon sites of the CTA<sup>+</sup> molecules.<sup>56</sup> As the CTA<sup>+</sup> species are the sole organic agents present in the aluminosilicate MCM-41a materials prepared under ambient conditions, all observed  $^1\text{H}$ – $^{13}\text{C}$  correlations arise from the structure-directing surfactant species.

In Figure 3, correlations are observed between single pairs of proton species and their respective carbon resonances. For short  $^1\text{H}$ – $^{13}\text{C}$  contact times in the pulse sequence, in practice less than ca. 10 ms, it is possible to measure only correlations between spatially adjacent species. For most of the HETCOR spectra to follow, short contact times have been used to preserve

(55) The symmetric, well-resolved  $^{13}\text{C}$  CPMAS signal for the CTA<sup>+</sup> headgroup in the ambient-prepared MCM-41a sample occurs at 54 ppm, the same as for CTA<sup>+</sup> in aqueous solution.<sup>56</sup> An identical spectrum is obtained for the hydrothermally prepared MCM-41h sample; the absence of a signal or shoulder at ~57 ppm (the solution phase  $^{13}\text{C}$  shift for TMA<sup>+</sup> species) indicates that TMA<sup>+</sup> counterions are not present in concentrations detectable by  $^{13}\text{C}$  NMR.

(56) Ulmius, J.; Lindman, B.; Lindblom, G.; Drakenberg, T. *J. Colloid Interface Sci.* **1978**, *65*, 88–97.

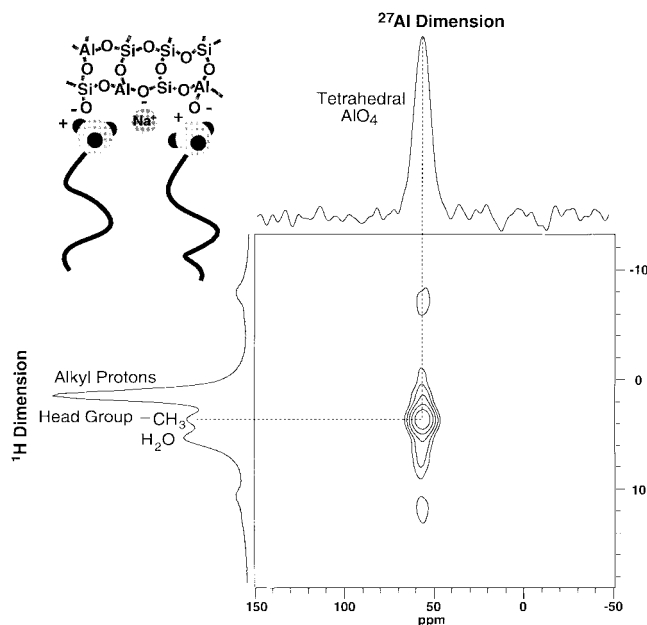


**Figure 4.** 2D  $^{27}\text{Al}\{^1\text{H}\}$  HETCOR spectrum for the same as-synthesized aluminosilicate MCM-41a sample used in Figure 3 (room temperature synthesis, molar Si/Al ratio of 8 in the initial reaction gel). Separate  $^{27}\text{Al}$  CPMAS and  $^1\text{H}$  MAS spectra are plotted along their corresponding axes. In the  $^{27}\text{Al}\{^1\text{H}\}$  HETCOR spectrum, tetrahedral aluminum species are correlated solely to the protons of the surfactant head group. Additional intensity can be observed from spinning sidebands in the  $^1\text{H}$  dimension; due to the scaling, these head group spinning sidebands are not visible in the 1D  $^1\text{H}$  MAS spectrum. The sidebands appearing in the  $^1\text{H}$  MAS spectrum along the vertical axis correspond to the more abundant  $-\text{CH}_2-$  species. Experimental Conditions: The sample was spun at 4.5 kHz; a 9.87- $\mu\text{s}$   $90^\circ$  pulse followed by a 1.5-ms contact time were used for cross-polarization. The 90° pulse length was assumed to be one-third of the 90° pulse length found for  $^{27}\text{Al}$  in aqueous solution.<sup>57,58</sup> The dwell time in  $t_1$  was 16.7  $\mu\text{s}$ , with the proton signals acquired off-resonance for phase sensitivity. The 1400 acquisitions with a 2-s recycle delay were acquired for each of the 68  $t_1$  increments. During the detection period ( $t_2$ ), 256 points were collected with a dwell time of 20.0  $\mu\text{s}$ . The first and second time domains were subsequently zero-filled to 512 points, and sinebell apodization and 500-Hz Gaussian line broadening were applied in  $t_1$  and  $t_2$ , respectively.

the advantage these measurements (Figure 1a) have for probing molecularly adjacent species in characterizing the structures of inorganic–organic interfaces. For longer contact times or if a mixing period is employed (Figure 1b), proton spin diffusion allows correlations to be observed between more weakly coupled species. By varying parameters such as the contact and mixing times in the HETCOR experiments, substantial control can be exerted over the threshold strength of the heteronuclear couplings measured.

**(b) Proton Correlations with Tetrahedral Aluminum and Silicon Species.** With the  $^1\text{H}$  peaks identified based on the 2D HETCOR spectrum in Figure 3, it is possible to correlate these resonances with those of nearby  $^{27}\text{Al}$  or  $^{29}\text{Si}$  species through their respective  $^1\text{H}$ – $^{27}\text{Al}$  or  $^1\text{H}$ – $^{29}\text{Si}$  dipolar couplings. By measuring correlations involving particularly protonated surfactant moieties, such couplings can be used to establish the presence of alumina and silica species at inorganic–organic interfaces in mesoscopically ordered MCM-41 materials. In Figure 4, separately acquired 1D  $^{27}\text{Al}\{^1\text{H}\}$  CPMAS and  $^1\text{H}$  MAS spectra are plotted along the horizontal and vertical axes, respectively, to aid in the analysis of the 2D  $^{27}\text{Al}\{^1\text{H}\}$  HETCOR spectrum obtained for the as-synthesized aluminosilicate MCM-

41a sample (prepared at room temperature using a molar Si/Al ratio of 8 in the starting reaction gel). The 1D  $^{27}\text{Al}$  CPMAS spectrum along the horizontal axis reveals a single  $^{27}\text{Al}$  peak (56 ppm, 10 ppm fwhm), whose chemical shift is consistent with aluminum species that are tetrahedrally coordinated through bridging oxygen atoms principally to silicon atoms.<sup>59</sup> In the contour plot of the 2D  $^{27}\text{Al}\{^1\text{H}\}$  HETCOR spectrum, the intensity profile shows clearly that, for a short 1.5-ms contact time, only the methyl  $^1\text{H}$  species on the surfactant head groups are correlated to the tetrahedral aluminum species. Low contour levels, ca. 10% of the spectral intensity, have been used to show that no intensity is observed in the region where hydroxyl resonances would be expected and to demonstrate that no detectable polarization transfer from the other  $^1\text{H}$  species is observed. This observation that the tetrahedral aluminum species are within ca. 1.0-nm dipole–dipole coupling distances to protons on the head groups of the structure-directing surfactant molecules indicates that these species are strongly interacting, consistent with the incorporation of aluminum atoms into the MCM-41a framework.

These results are corroborated by the  $^{29}\text{Si}\{^1\text{H}\}$  HETCOR spectrum shown in Figure 5 for the same as-synthesized MCM-41a sample; namely, that the silicate species of the aluminosilicate framework are also in close spatial proximity to protons associated with the surfactant head groups. One-dimensional  $^{29}\text{Si}\{^1\text{H}\}$  CPMAS and  $^1\text{H}$  MAS spectra accompany the 2D contour plot in Figure 5 along the horizontal and vertical axes, respectively. The  $^{29}\text{Si}\{^1\text{H}\}$  CPMAS spectrum shows a 2.3-kHz (fwhm) inhomogeneously broadened peak that spans the chemical shift range of partially and fully polymerized silica, including  $\text{Q}^2$ ,  $\text{Q}^3$ , and  $\text{Q}^4$  species, where the  $\text{Q}^n$  refers to tetrahedral silica units with  $n$  silicon next-nearest neighbors bonded through bridging oxygen atoms.<sup>59</sup> The 2D  $^{29}\text{Si}\{^1\text{H}\}$  HETCOR spectrum provides significantly increased spectral resolution showing that the protons from head group methyl species of the surfactant molecules (3.2 ppm) are correlated predominantly to  $\text{Q}^3$  silica species in the aluminosilicate framework. The absence in Figures 4 and 5 of appreciable coupling between hydroxyl/ $\text{H}_2\text{O}$  groups and framework aluminum or silicon species establishes that compensation of the anionic framework charges is dominated by the head groups of the  $\text{CTA}^+$  surfactant molecules. These experiments support the importance of charge-density matching across the inorganic–organic interface in the syntheses of M41S materials.<sup>6,27,60</sup> The essentially exclusive charge balancing role of the  $\text{CTA}^+$  head groups in this material differs from structural interpretations made for other MCM-41 samples based on 1D  $^{29}\text{Si}\{^1\text{H}\}$  CPMAS experiments and relaxation studies, in which significant concentrations of silanol groups were concluded to be present prior to removal of the surfactant species.<sup>61</sup> Structural differences, such as defect concentrations, among the samples may exist; however, the 2D methods discussed here possess significant correlative advantages over 1D NMR characterization strategies. In particular, the 2D HETCOR spectra in Figures 4 and 5 identify the  $\text{CTA}^+$  head groups, as opposed to hydroxyl species, as the specific and primary protonated source from which magnetization transferred

(57) Schmidt, V. H. *Pulsed Magn. Opt. Reson., Proc. Ampère Int. Summer School 1972*, 2nd, 75–83.

(58) Fenzke, D.; Freude, D.; Fröhlich, T.; Haase, J. *Chem. Phys. Lett.* **1984**, *111*, 171–175.

(59) Engelhardt, G.; Michel, D. *High-Resolution Solid State NMR of Silicates and Zeolites*; John Wiley & Sons: New York, 1987.

(60) Huo, Q.; Margolese, D. I.; Ciesla, U.; Feng, P.; Gier, T. E.; Sieger, P.; Leon, R.; Petroff, P. M.; Schüth, F.; Stucky, G. D. *Nature (London)* **1994**, *368*, 317–321.

(61) Steel, A.; Carr, S. W.; Anderson, M. W. *Chem. Mater.* **1995**, *7*, 1829–1832.

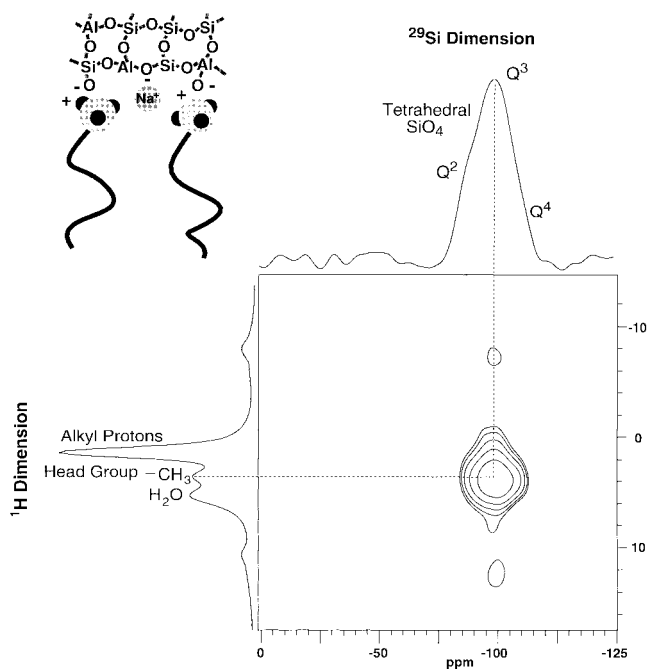


**Figure 5.** 2D  $^{29}\text{Si}\{^1\text{H}\}$  HETCOR spectrum for the aluminosilicate MCM-41a sample used in Figures 3 and 4. Separate  $^{29}\text{Si}$  CPMAS and  $^1\text{H}$  MAS spectra are plotted along their corresponding axes. In the  $^{29}\text{Si}\{^1\text{H}\}$  HETCOR spectrum, predominantly  $\text{Q}^3$  silica species are correlated to the trimethylammonium protons of the surfactant head groups. Low contour levels (ca. 10% of full intensity) are plotted to show clearly that the  $^1\text{H}$ – $^{29}\text{Si}$  cross-peak is centered at the  $^1\text{H}$  chemical shift for the head group methyl protons and to show the first set of spinning sidebands (SSB) in the  $^1\text{H}$  dimension. Experimental Conditions: The sample was spun at 4.5 kHz; a 12.0- $\mu\text{s}$   $90^\circ$  pulse followed by a 5.0-ms contact time were used for cross-polarization. The dwell time in  $t_1$  was 16.7  $\mu\text{s}$ , with the proton signals acquired off-resonance for phase sensitivity. The 800 acquisitions with a 2-s recycle delay were acquired for each of the 42  $t_1$  increments. During the detection period ( $t_2$ ), 512 points were collected with a dwell time of 20.0  $\mu\text{s}$ . The first and second time domains were subsequently zero-filled to 512 points, and sinebell apodization and 500-Hz Gaussian line broadening were applied in  $t_1$  and  $t_2$ , respectively.

to  $^{27}\text{Al}$  or  $^{29}\text{Si}$  framework species originates, thereby confirming their interfacial proximity to one another.

Following calcination and subsequent ion exchange with ammonium cations, the  $^{27}\text{Al}\{^1\text{H}\}$  HETCOR experiment was repeated to establish unambiguously the incorporation of aluminum species into the MCM-41a inorganic framework and to demonstrate the accessibility of the channels to charge-balancing cations in the resulting mesoporous solid material. Figure 6 displays the contour plot of the 2D  $^{27}\text{Al}\{^1\text{H}\}$  HETCOR spectrum for the calcined and ion-exchanged MCM-41a material, with the  $^{27}\text{Al}\{^1\text{H}\}$  CPMAS and  $^1\text{H}$  MAS spectra shown also along the horizontal and vertical axes, respectively. The 2D NMR spectrum in Figure 6 reveals that the tetrahedral aluminum peak is correlated strongly to the  $\text{NH}_4^+$  proton resonance at 6.9 ppm. The observance of such signal intensity in the contour plot reflects the existence of  $^1\text{H}$ – $^{27}\text{Al}$  dipolar couplings between charge-balancing ammonium cations and tetrahedral aluminum species in the calcined, ion-exchanged material. Thus, by locating the required surfactant head group or  $\text{NH}_4^+$  cations in the immediate molecular vicinity of the tetrahedral aluminum species, the  $^{27}\text{Al}\{^1\text{H}\}$  HETCOR experiments prove unequivocally that interfacial framework aluminum atoms have been incorporated into the as-synthesized MCM-41a material and that



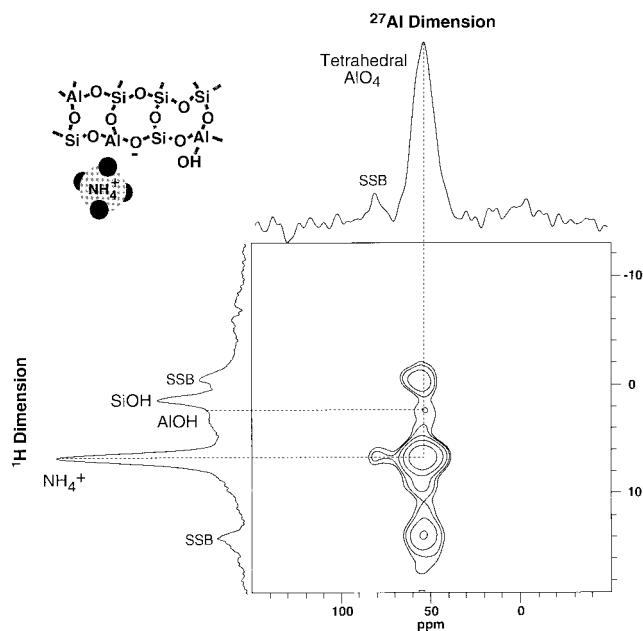


**Figure 6.** 2D  $^{27}\text{Al}\{^1\text{H}\}$  HETCOR spectrum for the calcined,  $\text{NH}_4^+$ -exchanged, and dehydrated aluminosilicate MCM-41a sample (synthesized at room temperature using a molar Si/Al ratio of 8 in the initial reaction gel).  $^{27}\text{Al}$  CPMAS and  $^1\text{H}$  MAS spectra are plotted along their corresponding axes. In this  $^{27}\text{Al}\{^1\text{H}\}$  HETCOR spectrum, correlations between the protons associated with the  $\text{NH}_4^+$  cations and the tetrahedral aluminum species are observed. In addition, a small peak appears in the 2D contour plot at 2.4 ppm in the  $^1\text{H}$  dimension that has been assigned to Lewis acid sites produced during the calcination. There does not appear to be a correlation between the protons associated with the silanol groups and the aluminum atoms in the inorganic framework. The remaining peaks in the 2D spectrum correspond to spinning sidebands. The conditions for this experiment were identical to those presented in Figure 4, with the exceptions that the sample was spun at 3.5 kHz and 2000 acquisitions were obtained for 64  $t_1$  increments.

framework aluminum species are preserved following calcination treatment.

In addition to the ammonium species observed for the calcined and  $\text{NH}_4^+$ -exchanged aluminosilicate MCM-41a material, the  $^1\text{H}$  MAS spectrum accompanying the 2D  $^{27}\text{Al}\{^1\text{H}\}$  contour plot along the vertical axis in Figure 6 shows a strong secondary signal at 1.6 ppm assigned to silanol (SiOH) protons.<sup>62</sup> A poorly resolved shoulder at 2.4 ppm is furthermore present in the range attributed to AIOH protons.<sup>62,63</sup> As previously noted in association with Figures 4 and 5, couplings associated with these hydroxyl species were not observed in the uncalcined material. The  $^{27}\text{Al}\{^1\text{H}\}$  HETCOR contour plot in Figure 6 shows that the  $^1\text{H}$  species producing the weak signal at 2.4 ppm appears to be correlated with the tetrahedral aluminum sites, consistent with their assignments to AIOH groups that may represent Lewis acid sites. An  $^1\text{H}$  signal near 2.4 ppm has been previously attributed to octahedrally coordinated extra-framework aluminum hydroxide species experiencing hydrogen-bonding interactions with the framework.<sup>62,63</sup> Only tetrahedrally coordinated aluminum, however, is observed for the aluminosilicate MCM-41a material examined here. The tetrahedral nature of the AIOH environments suggests that these aluminum species are incorporated covalently into the framework and are stabilized by neighboring silica species, although further spectroscopic investigations will be necessary to validate this assignment.

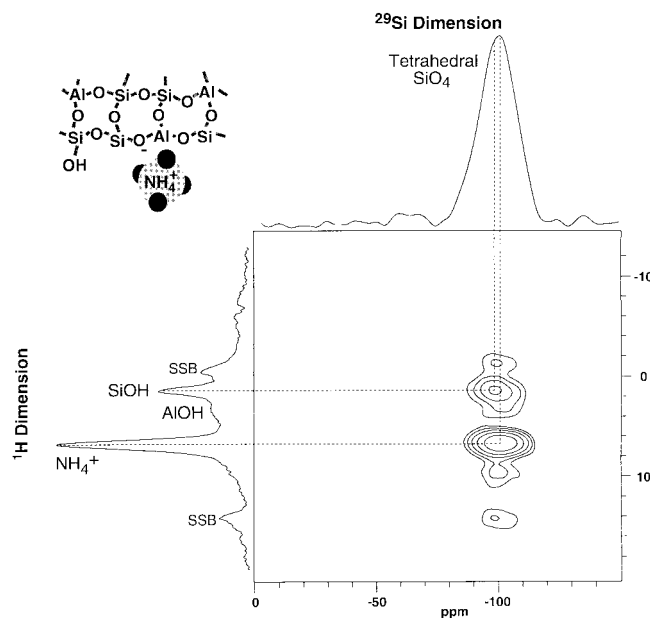


**Figure 7.** 2D  $^{29}\text{Si}\{^1\text{H}\}$  HETCOR spectrum for the same calcined,  $\text{NH}_4^+$ -exchanged, and dehydrated aluminosilicate MCM-41a sample used in Figure 6 (room temperature synthesis, molar Si/Al ratio of 8 in the reaction gel).  $^{29}\text{Si}$  CPMAS and  $^1\text{H}$  MAS spectra are plotted along their corresponding axes. In this  $^{29}\text{Si}\{^1\text{H}\}$  HETCOR spectrum, the  $^{29}\text{Si}$  resonances for  $\text{Q}^3$  silica species are clearly correlated to  $^1\text{H}$  signals from protons associated with silanol groups and  $\text{NH}_4^+$  cations. Additional peaks in the 2D contour plot correspond to spinning sidebands in the  $^1\text{H}$  dimension. Experimental Conditions: The sample was spun at 3.5 kHz; a  $9.5\text{-}\mu\text{s}$   $90^\circ$  pulse followed by a 10-ms contact time was used for cross-polarization. Shorter contact times did not appreciably change the spectrum, although the signal intensity was diminished. The dwell time during  $t_1$  was  $16.7\ \mu\text{s}$ , with the proton signals acquired off-resonance for phase sensitivity. The 2000 acquisitions with a 2-s recycle delay were acquired for each of the 65  $t_1$  increments. During the detection period ( $t_2$ ), 256 points were collected with a dwell time of  $50.0\ \mu\text{s}$ . The first and second time domains were subsequently zero-filled to 512 points, and sinebell apodization and 500-Hz Gaussian line broadening were applied in  $t_1$  and  $t_2$ , respectively.

Above this peak in the contour plot (Figure 6), the first spinning sideband from the intense ammonium proton signal appears in the  $^1\text{H}$  dimension, with no correlation observed between the silanol protons and the tetrahedral aluminum species. The absence of heteronuclear dipole–dipole coupling between SiOH protons (1.6 ppm) and the tetrahedral aluminum sites indicates that the silanol species in the calcined sample are not molecularly adjacent to the aluminum atoms in the MCM-41a framework. Such detailed structural information arises from the enhanced resolution provided by the 2D HETCOR experiment and reflects the utility of two-dimensional solid-state NMR techniques for correlating molecular proximities in these complicated heterogeneous systems.

The results for the  $^{27}\text{Al}\{^1\text{H}\}$  NMR studies of the calcined and  $\text{NH}_4^+$ -exchanged MCM-41a material are corroborated by the 2D  $^{29}\text{Si}\{^1\text{H}\}$  HETCOR spectrum shown in Figure 7. Chemical shift correlations are observed in the contour plot between tetrahedral silica species and both silanol and  $\text{NH}_4^+$  proton species. This is specifically evidenced by the intensity correlations between the  $\text{NH}_4^+$   $^1\text{H}$  peak (6.9 ppm) and the  $\text{Q}^3$  silica peak near  $-100$  ppm and between the silanol  $^1\text{H}$  peak (1.6 ppm) and what appears to be a different  $\text{Q}^3$  silica  $^{29}\text{Si}$  resonance at  $-98$  ppm. This distinction in the assignments of the silica species is based on the small but measurable difference

(62) Hunger, M. *Solid State Nucl. Magn. Reson.* **1996**, *6*, 1–29.

(63) Majjani, A.; Derouane, E. G.; Nagy, J. B. *Appl. Surf. Sci.* **1994**, *75*, 204–212.

in the positions of the two intensity correlations in the  $^{29}\text{Si}$  dimension of the 2D contour plot (Figure 7). Such enhancement of spectral resolution is reminiscent of the wideline separation (WISE) NMR experiment, which uses resolution of different carbon species to separate overlapping proton resonances;<sup>43</sup> however, in this case resolved proton resonances are used to separate overlapping  $^{29}\text{Si}$  signals from different  $\text{Q}^3$  silica species. Those tetrahedral  $\text{Q}^3$  silica species that are correlated with the charge-compensating  $\text{NH}_4^+$  cations (isotropic chemical shifts centered at  $-100$  ppm) are expected to be near framework aluminum atoms as next-nearest-neighbor species that are covalently bonded via bridging oxygen atoms. The other type of  $\text{Q}^3$  silica has one of its next-nearest-neighbor atoms replaced by a proton, forming silanol species that possess somewhat lower isotropic chemical shifts ( $-98$  ppm). The 2D HETCOR analysis reveals that the skewed  $^{29}\text{Si}$  lineshape in the 1D MAS spectrum results from two chemically distinct  $\text{Q}^3$  silica species and not from an asymmetric distribution of bond angles associated with a nominally single  $\text{Q}^3$  moiety within the aluminosilicate framework walls.

**(c) Proton Correlations with Octahedral Aluminum Species.** An important application of the  $^{27}\text{Al}\{^1\text{H}\}$  HETCOR experiment to M41S materials is to establish whether octahedrally coordinated aluminum species can be present within the aluminosilicate framework. As described above, a hexagonal mesostructured material (MCM-41h) was synthesized under hydrothermal conditions at  $100^\circ\text{C}$  with a molar Si/Al ratio in the initial reaction gel of 6.0. This synthesis procedure has been shown to result in octahedral aluminum species, and separate evaluations have indicated that these may be included in the MCM-41h inorganic framework.<sup>13</sup> Figure 8 shows the contour plot of the  $^{27}\text{Al}\{^1\text{H}\}$  HETCOR spectrum for this hydrothermally synthesized MCM-41h sample, with the 1D  $^{27}\text{Al}$  CPMAS and  $^1\text{H}$  MAS spectra plotted along their respective frequency axes. Similar to the MCM-41a material synthesized at room temperature (Figure 6), the 2D HETCOR spectrum of hydrothermally prepared MCM-41h in Figure 8 shows strong intensity correlations between the NMR peaks from tetrahedrally coordinated  $^{27}\text{Al}$  species (56 ppm) and the methyl protons attached to cationic ammonium groups (3.2 ppm), plus evidence of weaker  $^{27}\text{Al}$  couplings to protons of adsorbed water. For the hydrothermally prepared MCM-41h material, there is a strong additional correlation between six-coordinate  $^{27}\text{Al}$  species (6 ppm) and  $^1\text{H}$  nuclei associated with adsorbed water (4.7 ppm). This latter result establishes that a significant fraction of the octahedral aluminum species are dipole-dipole coupled and therefore in close spatial proximity to protons of bound water molecules.

On the basis of this information alone, however, it is not possible to ascertain whether the octahedrally coordinated Al species are a part of the MCM-41h inorganic framework. One means of resolving this is to look for evidence of couplings between the octahedrally coordinated Al species and protons associated with the structure-directing surfactant molecules. This is directly analogous to the results in Figure 4 for the MCM-41a sample prepared under ambient conditions, which show correlated signal intensities between tetrahedrally coordinated  $^{27}\text{Al}$  atoms and the methyl group protons of the  $\text{CTA}^+$  head groups. Unfortunately, however, attempts to measure weaker  $^1\text{H}-^{27}\text{Al}$  correlations using the standard HETCOR experiment (Figure 1a) with contact times longer than ca. 5 ms proved to be infeasible due to the shortness of the  $^{27}\text{Al}$   $T_{1\rho}$  relaxation times (which typically are on the order of several hundred microseconds).<sup>41,42</sup>

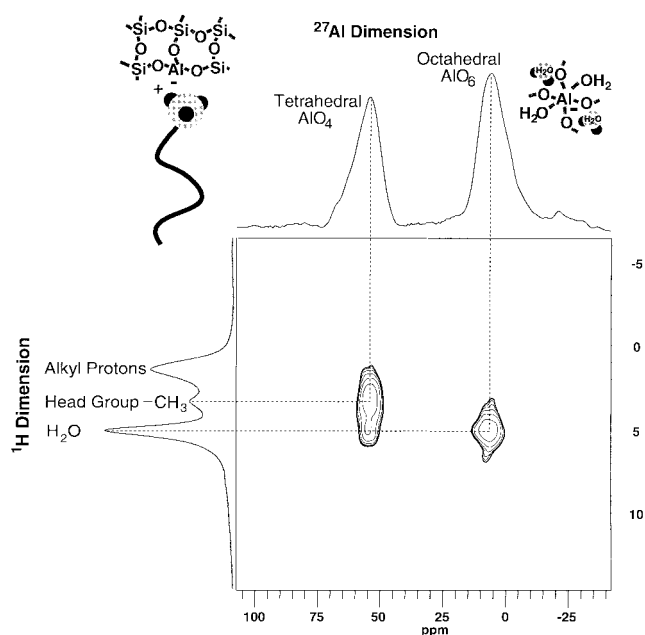


**Figure 8.** 2D  $^{27}\text{Al}\{^1\text{H}\}$  HETCOR spectrum for as-synthesized aluminosilicate MCM-41h prepared under hydrothermal conditions containing a Si/Al ratio of 6 in the initial reaction gel. Separate  $^{27}\text{Al}$  CPMAS and  $^1\text{H}$  MAS spectra are plotted along their corresponding axes. The peaks in the 2D contour plot indicate that the protons of the surfactant head group are strongly correlated to the tetrahedral aluminum species and also to adsorbed water. In addition, octahedrally coordinated aluminum species are present and correlated to adsorbed water. The experimental conditions for this experiment were identical to those presented in Figure 4, with the exceptions that the sample was spun at 3.5 kHz, 128 points were collected during  $t_2$ , 512 acquisitions were acquired for each of the 32  $t_1$  increments, and the data were acquired on resonance using TPPI phase cycling.

As discussed above, modification of the 2D HETCOR experiment to incorporate proton spin diffusion (Figure 1b) extends the range of observable  $^1\text{H}-^{27}\text{Al}$  correlations to include more weakly coupled species. Figure 9, for example, shows 2D spin-diffusion  $^{27}\text{Al}\{^1\text{H}\}$  HETCOR spectra acquired using mixing times of 15 and 25 ms, during which  $^1\text{H}$  magnetization is mixed among nearby proton species, prior to being transferred to Al atoms during the contact period. In Figure 9a, a mixing time of 15 ms shows correlated intensities in the 2D spin-diffusion  $^{27}\text{Al}\{^1\text{H}\}$  HETCOR spectrum between the  $^{27}\text{Al}$  peak (56 ppm) from tetrahedrally coordinated aluminum atoms and resolved signals from each of the different proton species, including adsorbed water and the head group and alkyl chain moieties of the  $\text{CTA}^+$  surfactant molecules. Intensity correlations are also observed between the  $^{27}\text{Al}$  peak at 6 ppm associated with the octahedral aluminum sites and the  $^1\text{H}$  peaks from adsorbed water and ammonium methyl groups associated with the surfactant head groups.<sup>64</sup> Interfacial interactions between the structure-directing surfactant molecules and the octahedral aluminum can be confirmed by measuring  $^1\text{H}-^{27}\text{Al}$  correlations involving the alkyl surfactant chain protons, which distinguish the  $\text{CTA}^+$  species from the  $\text{TMA}^+$  cations (Figure 9). In fact, correlations between octahedral Al sites and weakly coupled alkyl species are observed when a longer mixing time ( $t_{\text{mix}} = 25$  ms) is used, as shown in the HETCOR spectrum of Figure 9b. The appearance of such correlations involving protons on the alkyl surfactant chain establish the presence of

(64) Raman and  $^{13}\text{C}$  NMR<sup>55</sup> results show no evidence for the incorporation of  $\text{TMA}^+$  base cations into the as-synthesized MCM-41h product.



material as a function of sample hydration. A  $^1\text{H}$  spin-diffusion  $^{27}\text{Al}\{^1\text{H}\}$  HETCOR experiment (not shown here) performed on the as-synthesized MCM-41h sample after partial dehydration (at 60 °C for 72 h) to remove weakly bound water revealed intensity correlations between the octahedrally coordinated aluminum species and the  $\text{CTA}^+$  surfactant head groups at significantly shorter mixing times ( $t_{\text{mix}} = 5$  ms) than observed in Figure 9 ( $t_{\text{mix}} = 15$  ms). Whereas the  $^{27}\text{Al}$  CPMAS spectrum of the partially dehydrated sample remained unchanged from those in Figures 8 and 9 above, removal of the weakly adsorbed water leads to significantly diminished spectral resolution in the proton dimension.<sup>68</sup> This is due to stronger homonuclear  $^1\text{H}$ – $^1\text{H}$  dipole–dipole couplings that exist among the strongly adsorbed water and surfactant species that remain in the partially dehydrated sample. Such  $^1\text{H}$ – $^1\text{H}$  couplings have been shown to exist among the adsorbed water and surfactant species by separate 2D  $^1\text{H}\{^1\text{H}\}$  homonuclear chemical shift correlation experiments (see Supporting Information).<sup>69</sup> Upon rehydration, the 1D and 2D  $^1\text{H}$  and  $^{27}\text{Al}$  spectra are restored in appearance to those shown in Figures 8 and 9, demonstrating the reversibility of physical or weak chemical adsorption of water under these mild conditions.

Thus, analyses of both Figures 8 and 9 establish unambiguously that protons associated with the surfactant species are dipole–dipole coupled to both tetrahedrally and octahedrally coordinated  $^{27}\text{Al}$  atoms at what appears to be a common inorganic–organic interface. The close proximity of the structure-directing surfactant molecules to both four- and six-coordinate aluminum species in the hydrothermally prepared aluminosilicate MCM-41h sample reflects framework locations for both the tetrahedral and octahedral Al sites. This situation, in fact, is distinct from 2D  $^{27}\text{Al}\{^1\text{H}\}$  HETCOR results (not shown here) measured on a physical mixture of as-synthesized MCM-41a and pseudo-boehmite powders, which possess exclusively tetrahedrally and octahedrally (entirely nonframework) coordinated aluminum species, respectively. The tetrahedral and octahedral Al sites in each of the ca. 10  $\mu\text{m}$  MCM-41a or pseudo-boehmite particles are macroscopically separate. Similar to Figure 4, the HETCOR measurements on a physical mixture of these powders showed the protons associated with the surfactant head groups to be correlated with four-coordinate  $^{27}\text{Al}$  atoms in the aluminosilicate MCM-41a materials. However, as expected, no similar correlations were observed either directly or indirectly between the surfactant species and the octahedrally coordinated Al sites in the pseudo-boehmite crystallites. These results provide coarse verification of the sensitivity and selectivity of the 2D NMR experiments for identifying framework  $^{27}\text{Al}$  sites that are dipole–dipole coupled to protons associated with organic surfactant species.

The HETCOR measurements support the conclusions that both four- and six-coordinate Al species are present in the framework of the hydrothermally synthesized MCM-41h sample. This, in fact, may be similar to what has been observed in nanoporous crystalline aluminophosphates, where certain tetrahedral framework aluminum sites have been shown to interact strongly with adsorbed water, such that they achieve octahedral coordination.<sup>33–35</sup> These results support earlier work, which suggested that hydrothermal preparations of aluminosilicate MCM-41 materials could lead to octahedral aluminum environ-

ments produced by strong interactions between framework Al species and adsorbed water or surfactant molecules in the mesoporous channels.<sup>13</sup> Work is currently in progress in our laboratory to probe whether weak  $^{29}\text{Si}$ – $^{27}\text{Al}$  dipolar couplings can be measured, the existence of which would confirm the incorporation of octahedrally coordinated aluminum species into the MCM-41 frameworks of hydrothermally synthesized materials.

## Conclusions

Two-dimensional chemical shift correlation NMR provides a powerful solid-state spectroscopic tool for identifying adjacent molecular species using through-space heteronuclear dipolar couplings. The results presented here are the first to characterize interfacial structures and to establish unambiguously the incorporation of aluminum species in as-synthesized and calcined aluminosilicate MCM-41 mesophase solids. This is achieved by demonstrating that polarization transfer occurs between structure-directing organic molecules or exchangeable cations and  $^{27}\text{Al}$  or  $^{29}\text{Si}$  nuclei associated with inorganic oxide species of the mesophase framework. By exploiting the dipolar couplings between protons associated with ionic or adsorbed molecules and neighboring  $^{27}\text{Al}$  or  $^{29}\text{Si}$  nuclei, interfacial species can be identified and their local structure probed. As shown for the case of aluminum incorporation in MCM-41 materials, framework substitution of heteroatoms (particularly NMR-active species) is especially amenable to such investigations. These studies in combination with complementary techniques, such as powder X-ray diffraction and elemental analysis, establish a firm basis for identifying aluminum incorporation into the frameworks of mesoporous molecular sieves and for locating specific chemical species at inorganic–organic interfaces. This approach is expected to be generally applicable to the study of interfacial structures at a molecular level in a wide range of heterogeneous composite systems, including zeolites, inorganic–organic mesophases, mesoporous materials, and biominerals.

**Acknowledgment.** We thank Prof. C. Jäger, Prof. K. T. Mueller, and Dr. F. Babonneau for helpful discussions and also one of the anonymous reviewers for thoughtful comments. This work was supported by the NSF Young Investigator Program (B.F.C.), the David and Lucile Packard Foundation (B.F.C.), Shell Research B.V. (B.F.C.), and NSF Grant DMR-9520971 (G.D.S.). The experiments were conducted on NMR instrumentation supported in part by the NSF Division of Materials Research under Grant DMR-9222527 and through the UCSB Materials Research Laboratory under Award DMR-9632716. M.T.J. acknowledges support from the Biotechnology Research and Education Program of the University of California. S.C.C. is supported by funding from the U.S. Army Research Office under Grant DAAH04-96-1-0443. B.F.C. is a Camille and Henry Dreyfus Teacher-Scholar and an Alfred P. Sloan Research Fellow.

**Supporting Information Available:** A 2D  $^1\text{H}\{^1\text{H}\}$  homonuclear chemical shift correlation NMR spectrum acquired for the hydrothermally synthesized MCM-41h sample showing the existence of  $^1\text{H}$ – $^1\text{H}$  couplings between protons associated with the surfactant head groups, alkyl chains, and adsorbed water (3 pages, print/PDF). See any current masthead page for ordering information and Web access instructions.

(68) Christiansen, S. C. Ph.D. Dissertation, Dept. of Chemical Engineering, University of California at Santa Barbara, Manuscript in preparation.

(69) Janicke, M. T. Ph.D. Dissertation, Dept. of Chemical Engineering, University of California at Santa Barbara, 1997.